BINGHAM FLUID FLOW IN THE ENTRANCE REGION OF A PIPE

by

Basma Mokhtar Hussein Mohamed Baioumy

A Thesis presented to the Faculty of the
American University of Sharjah
College of Engineering
In Partial Fulfillment
of the Requirements
for the Degree of

Master of Science in
Chemical Engineering

Sharjah, United Arab Emirates

May 2019

Approval Signatures

We, the undersigned, approve the Master's Thesis of Basma Mokhtar Hussein Mohamed Baioumy.

Thesis Title: Bingham Fluid Flow in the Entrance Region of a Pipe

Signature	**Date of Signature** (dd/mm/yyyy)
_____	_____
Dr. Rachid Chebbi Professor, Department of Chemical Engineering Thesis Advisor	
_____	_____
Dr. Nabil Abdel Jabbar Professor, Department of Chemical Engineering Thesis Co-Advisor	
_____	_____
Dr. Mohamed Gadalla Professor, Department of Mechanical Engineering Thesis Committee Member	
_____	_____
Dr. Zarook Shareefdeen Professor, Department of Chemical Engineering Thesis Committee Member	
_____	_____
Dr. Sameer Al-Asheh Head, Department of Chemical Engineering	
_____	_____
Dr. Lotfi Romdhane Associate Dean for Graduate Affairs and Research College of Engineering	
_____	_____
Dr. Naif Darwish Professor and Acting Dean, College of Engineering	
_____	_____
Dr. Mohamed El-Tarhuni Vice Provost for Graduate Studies	

Acknowledgement

I thank my advisors, Dr. Rachid Chebbi and Dr. Nabil Abdel Jabbar, for their support, guidance and encouragement throughout the preparation of the study.

I would also like to thank the professors of the Chemical Engineering department who provided academic and professional counselling.

Finally, I would like to thank the American University of Sharjah for providing me with a graduate teaching assistantship, quality education, quality services and generous support to research and development.

Dedication

To my family and friends…

Abstract

The isothermal laminar flow of a Bingham fluid in the entrance region of a circular pipe has been studied previously by many authors using different approaches. As current research stands, the momentum integral approach provides analytical results that do not match the boundary-layer thickness experimental data for Newtonian fluid flow. No experimental data is currently available for the velocity profiles in the entrance region for Bingham fluids. The objective of this investigation is to determine the entrance region length in addition to the velocity and pressure profiles in the entrance region using a modified momentum integral method that improves the previously published boundary-layer model. The present work results reach asymptotically the fully developed values and show good agreement with published experimental data for pressure drop in the entrance region. The results are also in good agreement with the boundary-layer thickness experimental data for Newtonian fluid flow.

Keywords: ***Non-Newtonian; Bingham; Entrance Region; Momentum Integral Method.***

Table of Contents

List of Figures

List of Tables

Nomenclature

C_f	Skin-friction coefficient
p	pressure
p_0	pressure at the entry
p*	dimensionless pressure, $p/(\rho U_o^2/2)$
p_0*	dimensionless pressure at the entry, $p_0/(\rho U_o^2/2)$
$\|\Delta p^*\|$	dimensionless pressure drop, p_0*- p*
R	pipe radius
r	radial coordinate
r_1	dimensionless radial coordinate, r/R
r_o	plug-flow radius
r_o*	dimensionless plug-flow radius, r_o/R
r_e*	dimensionless developed plug-flow radius (r_e*= r_o* beyond the inlet region)
Re	Reynolds number, $(2R)U_o\rho/\mu_0$
U_∞	core velocity
U_c	centerline velocity ($U_c = U_\infty$ in the inlet region)
U_o	average velocity
U_c*	dimensionless centerline velocity, U_c/U_o ($U_c = U_\infty$ in the inlet region)
$U_{c,fd}$*	dimensionless fully developed centerline velocity
u	z component of the velocity
$\bar{u}$	dimensionless z-component of the velocity, u/U_c ($U_c = U_\infty$ in the inlet region)
u_o	fully developed z-component of the velocity in the outer flow region
u_i	fully developed z-component of the velocity in the inner plug-flow region
v	r-component of the velocity
y	R – r
z	axial distance

Greek Letters

η	dimensionless y, y/ δ
ξ	dimensionless axial distance, z/(Re R)
ξ_e	dimensionless entrance region length
δ	boundary layer thickness
δ_1	dimensionless boundary-layer thickness, δ/R
δ_e	dimensionless developed boundary-layer thickness ($\delta_e = \delta_1$ beyond the inlet region)
δ^*	displacement thickness
δ^{**}	momentum thickness
δ_1^*	dimensionless displacement thickness
δ_1^{**}	dimensionless momentum thickness
ρ	density
μ_0	Bingham viscosity
$\boldsymbol{\tau}$	shear stress tensor
τ_0	yield stress
τ_1	dimensionless Bingham number, $\tau_0^* \delta_1^3/(1- \delta_1)U_0/U_c$ ($U_c = U_\infty$ in the inlet region)
τ_2	dimensionless Bingham number, $6*\tau_1/(6+ \delta 1)$
τ_w	wall shear stress
τ_0*	Bingham number, $\tau_0 R/ \mu_0 U_o$
λ	pressure gradient parameter, $\delta^2\rho/\mu_0 \, dU_c/dz$ ($U_c = U_\infty$ in the inlet region)
λ_1	dimensionless pressure gradient parameter, $6(\lambda- 2\delta_1)/ 6+\delta_1$
Γ	second pressure gradient parameter, $\delta^2/U_\infty(\partial^2 u/\partial^2 r)_{r=ro}$
Γ_1	dimensionless second pressure gradient parameter, $\Gamma/6+\delta_1$

Chapter 1. Introduction

1.1. Overview

Laminar flow in entrance region length, i.e. the length required for fluids to become "fully-developed", has been studied extensively for various types of fluids. Recent works can be found in [1-5]. Finding the velocity of fluids in the entrance region of a pipe is important in cases where the total pipe length is not large, such as in compact heat exchanger design or short tubes leading to a diffuser or a nozzle [6]. The focus of the present study is on the problem of Bingham fluid flow in a circular pipe.

Bingham fluids, also known as Bingham plastics, act like a solid under small shear stresses, and the fluid has infinite viscosity until certain critical yield stress is reached. Beyond the yield stress, the apparent viscosity is finite. Several fluids used in the industry are non-Newtonian including various suspensions such as coal–water or coal-oil slurries, glues, inks, polymer solutions and others [7]. The fluid considered here is the Bingham model, which is of the 'time-independent yield stress' fluid category. The following Bingham model is the simplest model used to describe the behavior of such fluids [9].

$$\tau = \tau_0 - \mu_0 \frac{\partial u}{\partial r} \tag{1.1}$$

$$\partial u / \partial r = 0 \text{ when } \tau \leq \tau_0 \tag{1.2}$$

τ is the shear stress, τ_0 is the yield stress and μ_0 is the Bingham viscosity. Table 1 shows some experimental values for some fluids that follow this model.

Table 1.1: Parameters for Bingham Plastics [9].

Material	Temperature (^oC)	Yield Stress τ_0 (Pa)	Plastic viscosity μ_0 (kg/m.s)
Mayonnaise	30	85	0.63
Toothpaste	20	200	10
Paint	20	8.7	0.095

1.2. Thesis Objectives

To investigate the entrance length, velocity and pressure profiles of a Bingham plastic fluid in the entrance region of a circular pipe, using a momentum integral method while including not only the inlet region, but also the filled region.

1.3. Research Contribution

The proposed investigation provides enrichment to Karman's momentum integral method by accounting for the existence of the filled region as part of the entrance region. The method and model results are compared with available models.

1.4. Thesis Organization

Chapter 2 presents previous research addressing this problem and introduces the fundamental theory of Bingham fluid flow in a circular pipe. Chapter 3 presents the methodology and derivations using the momentum integral method. The results are presented, discussed and compared with previous works in Chapter 4. Chapter 5 concludes the study.

Chapter 2. Background and Literature Review

Several studies have investigated the entrance region length both analytically and numerically, but only recently have accurate results become available for Newtonian and non-Newtonian inelastic fluids obeying the power-law model [8]. In this section, all previous investigations for the entrance region length of a Bingham fluid will be reviewed. To begin with, the boundary layer theory which is of significant historical importance will be discussed.

2.1. The Boundary Layer Theory

In the late 19th century, fluid mechanics investigators were divided into two fundamental groups in terms of their attempt to solve engineering problems: hydrodynamicists who used the conservation principles and hydraulicians used empirical equations. To facilitate solutions, hydrodynamicists theorized a perfect fluid with zero viscosity and constant density. Even though these solutions were valid for flows that did involve solid surfaces, they did not solve more relevant engineering problems concerning fluid behavior in pipes and channels. A wit of the period said, "Hydrodynamicists calculate that which cannot be observed; hydraulicians observe that which cannot be calculated" [9].

Ludwig Prandtl's introduction of the boundary layer concept in 1904 helped to bring the two groups together. The boundary layer conceptually divides the flow into two parts: a much smaller region close to the solid surface where viscous effects are too large to be ignored, and the region outside the boundary layer where viscous effects are negligible. At the edge of the boundary layer, the solutions of the velocities and pressure must be matched. Prandtl also suggested that the point where the z-component of the velocity reaches 0.99 times the free-stream velocity marks the edge of the boundary layer. Even though this division is not a physically observed boundary, this concept provides a better intellectual basis for discussing flows than had previously existed [9].

For a steady, laminar flow with constant density and viscosity, the following simplifications of the conservation of mass and momentum equations are made in the boundary layer region where v_x and v_y are the x and y components of the velocity, respectively, and p is the pressure.

1- Two dimensions for the flow

2- $\frac{dp}{dy}$ is negligible

3- $\frac{\partial^2 v_x}{\partial x^2} << \frac{\partial^2 v_x}{\partial y^2}$ and is neglected

The above simplifications led to the boundary layer equations or Prandtl's boundary layer equations for Newtonian fluids [10].

$$\frac{\partial v_x}{\partial x} + \frac{\partial v_y}{\partial y} = 0 \tag{2.1}$$

$$v_x \frac{\partial v_x}{\partial x} + v_y \frac{\partial v_y}{\partial y} = -\frac{1}{\rho}\frac{dp}{dx} + \frac{\mu}{\rho}\frac{\partial^2 v_x}{\partial y^2} \tag{2.2}$$

2.2. Previous Investigations

This concept can be utilized to describe Bingham fluid flow in a circular pipe. When the concerned fluid enters a horizontal pipe, a velocity boundary layer and a shear boundary layer exist [11]. The thickness of these boundary layers gradually increases from zero as we move in the direction of fluid flow until it reaches a limiting value, depending on the characteristic yield stress. In this inlet region, the velocity profile is still developing, and thus the flow is called developing flow. At the edges of their respective boundary layers, the velocity and shear stress gradients are zero, and the fluid flows in "plug-flow" characteristic of Bingham fluids. Beyond the inlet region, the velocity profile in [11] is considered fully developed with the centerline velocity reaching the fully developed velocity profile predicted. The first region is considered as the entrance region, while the latter as the fully developed region [11]. The analysis was performed using a parabolic approximation profile [11].

Restriction of the entrance region to the inlet region does not allow for smooth matching of the velocity profile since the velocity gradient does not approach zero. To resolve this issue, Ishizawa [12] proposed that the entrance region be divided into two parts, inlet and filled regions for fluid flow in a pipe [13]. The previously defined entrance region is the inlet region. In the inlet region, viscous effects are accounted for within the boundary layer only. However, in the filled region, the whole fluid across the pipe section is influenced by viscous effects. At the end of the inlet region, the

boundary layer meets with the corresponding plug-flow radius, but the velocity profile is not yet fully developed. The fully developed viscous profile is reached asymptotically at the end of the filled region. This approach was successfully implemented by Mohanty et al. [13] and Chebbi [14] for Newtonian fluids and power-law fluids, respectively.

The earliest study to find the entrance length for a Bingham fluid was done by Michiyoshi et al. [15]. The variational method used had several major inconsistencies as analyzed by Chen et al. [11]. The assumptions made were unrealistic leading to the doubtful equation of motion, and the proposed velocity profile would not represent the flow behavior of Bingham fluids. Chen et al. [11] analyzed the problem, using two different analytical methods: the momentum integral method by Schiller [16] which employed a pre-assumed parabolic velocity profile and the Campbell-Slattery method [17]. Both methods were initially devised to solve problems for Newtonian fluids. The first method led to unrealistic results far from a small region near the inlet ($z^*>0.04$ where z^* is the dimensionless axial distance, $z/(Re^*R)$). The second method uses a macroscopic mechanical energy balance to account for viscous dissipation and generally provides a more accurate overall description of flow characteristics of Bingham fluids in the entrance region [11]. For fluids with different yield stresses, the methods provide significantly varying estimates of the entrance length.

Shah et al. [18] were the first to approach the solution to this problem numerically using the Patankar and Spalding procedure [19] and to produce results that are comparable to the ones achieved by the Campbell-Slattery method. The Campbell-Slattery method proved to be much more consistent with their results than the momentum integral balance. The results of Shah et al., with a yield stress of zero, are in agreement with previous work done for Newtonian fluids and the fully developed region for all yield numbers. Therefore, this adds validity to their work [18].

Nowak et al. [20] approached the problem using a macroscopic mass and momentum balance. They used the approach devised by Matras et al. [21] for the Newtonian case where the velocity profile is not pre-assumed but rather determined using overall mass and momentum balances at different locations from the inlet. Their results are intermediate between those obtained with the momentum-integral and Campbell-Slattery methods except for low values of the Bingham number [20].

Vradis et al. [22] were the first to provide a numerical solution for the simultaneous developing hydrodynamic and temperature fields in a pipe by discretizing the governing continuity, momentum and energy equations into a system of finite difference equations. They used the equation of momentum in all 3 co-ordinates (r, Θ, z) to study both the hydrodynamic and thermal effects in the entrance region. They argued that boundary layer equations completely fail to predict the actual flow characteristics due to the oversimplification of a uniform pressure gradient [22].

Finally, Poole et al. [23] present a detailed numerical study which reconciles issues in previous numerical work and believe that the uncertainty in their estimated entrance length is no more than 2%. Poole et al. [23] argued that all previous work done, except for Ookawara et al. [24] for circular geometry and Al Khatib et al. [25] for semi-infinite channels (bi-viscosity model), is entirely inaccurate. All previous work done for circular tube geometry ignored the diffusion dominated case (i.e. low Reynolds number), and thus incorrectly predicts that for creeping flows, the velocity instantaneously develops [23]. To overcome that, Ookawara et al. [24] "redefined the entry length as the axial distance, where the velocity at a radial position of 95% of the plug radius reaches 99% of the calculated maximum velocity (at the same radial location)". Poole et al. [23] also point out that Ookawara's correlation, which is independent of Bingham number, seems unrealistic, especially for low Reynolds number, given previous results for the power-law model. Therefore, Poole et al. chose to compare their final results with the analytical solution for fully developed flow and obtained excellent agreement [23].

As current research stands, the analytical momentum integral solution using the boundary layer theory by Chen at al. [11] for Bingham fluids deviates significantly from all other works done. On the other hand, the boundary layer theory implemented by Mohanty and Asthana [13] for Newtonian fluid flow and Chebbi [14] for power-law fluids in a pipe proved to be successful. This suggests that the defect is not in theory, but in implementation.

Chapter 3. Methodology

In this study, we investigate the flow of a Bingham fluid in a circular pipe of radius R. The following assumptions are made: steady-state, laminar flow, isothermal conditions, and constant physical properties. The governing continuity, momentum and constitutive equations in cylindrical coordinates for both the inlet and filled regions reduce to

$$\frac{1}{r}\frac{\partial}{\partial r}(rv) + \frac{\partial}{\partial z}(u) = 0 \tag{3.1}$$

$$v\frac{\partial u}{\partial r} + u\frac{\partial u}{\partial z} = -\frac{1}{\rho}\frac{dp}{dz} - \frac{1}{\rho r}\frac{\partial}{\partial r}(r\tau_{rz}) \tag{3.2}$$

$$\tau_{rz} = \tau_0 - \mu_0\frac{\partial u}{\partial r} \tag{3.3}$$

where r and z are the radial and axial coordinates, respectively, u and v are the velocity components in the z and r directions, respectively, p is the pressure, τ_{rz} is the shear stress in the z direction on a unit area perpendicular to the r direction, τ_0 is the yield stress, and μ_0 is the Bingham viscosity.

As fluid enters a horizontal pipe, the boundary layer thickness gradually increases downstream from zero until it reaches a limiting value depending on the characteristic yield stress. In the core region, there is "plug-flow" characteristic of Bingham fluids [11]. The plug-flow radius is related to the yield stress [11] by

$$\tau_0^* = \frac{12r_e^*}{3 - 4r_e^* + r_e^{*4}} \tag{3.4}$$

where τ_0^* is the dimensionless yield stress which is related to the Bingham number (Y = $2\tau_0^*$) and r_e^* is the dimensionless plug-flow radius for the fully-developed flow. As r_e^* approaches zero, i.e. no plug-flow exists, the boundary layers meet at the pipe axis, and the fluid is Newtonian. At the end of the inlet region, the fully developed plug-flow radius is reached. In the filled region, the plug-flow radius remains constant, and the fully-developed velocity profile is reached asymptotically at the end of the filled region. This section outlines the derivations of all the equations used to solve this problem.

3.1. Conservation of Mass

Applying an overall mass balance yields the following equation:

$$\left[\int_0^R u\, r dr\right]_{in} = \left[\int_0^R u\, r dr\right]_{out} \tag{3.5}$$

The average velocity can be written as

$$U_o \equiv \int \frac{u}{A} dA = \frac{2}{R^2}\int_0^R u\, r dr \tag{3.6}$$

Combining the above two equations gives

$$\frac{U_o R^2}{2} = \int_0^R U_c\, r dr - \int_{R-\delta}^R U_c\, r dr + \int_{R-\delta}^R u\, r dr \tag{3.7}$$

$$\frac{U_o R^2}{2} = \frac{U_c R^2}{2} - \int_{R-\delta}^R (U_c - u) r dr \tag{3.8}$$

Rearranging equation (3.8) and changing the integration variable to y, where y = R – r is the distance from the wall, yields

$$\frac{R^2}{2}(U_c - U_o) = U_c R \int_o^\delta \left(1 - \frac{u}{U_c}\right)\left(1 - \frac{y}{R}\right) dy \tag{3.9}$$

Using the following definition from Mohanty et al. [13] for the displacement thickness

$$\delta^* \equiv \int_0^\delta \left(1 - \frac{u}{U_c}\right)\left(1 - \frac{y}{R}\right) dy \tag{3.10}$$

equation (3.9) can be expressed in terms of the displacement thickness as

$$\frac{U_o}{U_c} = 1 - \frac{2\delta^*}{R} \tag{3.11}$$

Equation (3.11) can be differentiated with respect to z to yield

$$\left(1 - \frac{2\delta^*}{R}\right)\frac{dU_c}{dz} + U_c\left(-\frac{2}{R}\right)\frac{d\delta^*}{dz} = 0 \tag{3.12}$$

The following dimensionless variables can be used

$$Re = \frac{\rho U_0 (2R)}{\mu_0} \qquad \delta_1 = \frac{\delta}{R} \qquad \delta_1^* = \frac{\delta^*}{R} \qquad \xi = \frac{z}{R\, Re} \tag{3.13}$$

and substituting in the above equation, results in the following ordinary differential equation:

$$\frac{d\delta_1^*}{d\xi} = \left(1-2\delta_1^*\right)\frac{\lambda}{\delta_1^2}\left(\frac{U_o}{U_c}\right) \tag{3.14}$$

3.2. Governing Equations in the Inlet Region

3.2.1. Boundary conditions in the inlet region. The problem's boundary conditions are defined as:

B.C. 1: at $y = 0$ $\quad u = v = 0$

$\quad u = U_\infty(z)$

B.C. 2: at $y = \delta$

B.C. 3: at $y = \delta$ $\quad \frac{\partial u}{\partial y} = 0$

B.C. 4: at $y = \delta$ $\quad \frac{\partial^2 u}{\partial y^2} = 0$ (3.15)

where $U_\infty(z)$ is the potential core velocity, δ is the boundary layer thickness, and y is the distance from the pipe wall ($y = R - r$).

In addition, we define $\Gamma(z)$ and $\lambda(z)$ as

$$\Gamma = \frac{\delta^2}{U_\infty}\left(\frac{\partial^2 u}{\partial r^2}\right)_{r=r_0} \tag{3.16}$$

$$\lambda = \delta^2 \frac{\rho}{\mu_0}\frac{dU_\infty}{dz} \tag{3.17}$$

which extends the definitions used by Mohanty et al. [13] to Bingham fluid flow. Γ is zero in the inlet region.

Applying the momentum equation (3.2) at the wall yields

$$\left[\frac{1}{\rho r}\frac{\partial}{\partial r}(r\tau_{rz})\right]_{r=R} = -\frac{1}{\rho}\frac{dp}{dz} \tag{3.18}$$

Applying equation (3.2) at the edge of the boundary layer gives

$$-\frac{1}{\rho}\frac{dp}{dz} = U_\infty\frac{dU_\infty}{dz} + \frac{\tau_0}{\rho\, r_0} \tag{3.19}$$

which is similar to the one derived in Section 3.2.2. Using the above two equations and applying the definition of λ, we get the last boundary condition

B.C.5: at $y = 0$ $\quad \lambda = \delta_1\frac{\partial \bar{u}}{\partial \eta} - \frac{\partial^2 \bar{u}}{\partial \eta^2} - \tau_1;$

$$\bar{u} = \frac{u}{U_\infty}, \quad \eta = \frac{y}{\delta}, \quad \delta_1 = \frac{\delta}{R}, \tau_1 = \frac{\tau_o{}^* \delta_1{}^3}{(1-\delta_1)} \frac{U_o}{U_\infty}. \tag{3.20}$$

3.2.2. Pressure gradient in the inlet region. Applying the momentum equation (3.2) at the edge of the boundary layer yields

$$U_\infty \frac{dU_\infty}{\partial z} = -\frac{1}{\rho}\frac{dp}{dz} - [\frac{1}{\rho r}\frac{\partial}{\partial r}(r\tau_{rz})]_{r=r_o} \tag{3.21}$$

Simplifying the above equation by using the definition of τ_{rz} from equation (3.3) yields the pressure gradient profile in the inlet region.

$$-\frac{1}{\rho}\frac{dp}{dz} = U_\infty \frac{dU_\infty}{\partial z} + \frac{\tau_0}{\rho\, r_0} \tag{3.22}$$

3.2.3. Integral form of the governing equation in the inlet region. The von Kármán-Pohlhausen scheme is used to obtain the solution of the boundary layer equation. Substituting equation (3.22) into (3.2) results in

$$u\frac{\partial u}{\partial z} + v\frac{\partial u}{\partial r} = U_\infty \frac{dU_\infty}{dz} + \frac{\tau_0}{\rho\, r_0} - \frac{1}{\rho r}\frac{\partial}{\partial r}(r\tau_{rz}) \tag{3.23}$$

Rearranging equation (3.1) and substituting into the above equation gives

$$u\frac{\partial u}{\partial z} + \left(-\frac{1}{r}\int_0^r \frac{\partial u}{\partial z} r dr\right)\frac{\partial u}{\partial r} = U_\infty \frac{dU_\infty}{dz} + \frac{\tau_0}{\rho\, r_0} - \frac{1}{\rho r}\frac{\partial}{\partial r}(r\tau_{rz}) \tag{3.24}$$

The next step is to integrate from r = R at the wall to R = R - δ at the edge of the boundary layer. Integrating the 2nd term using integration by parts gives

$$\int_R^{R-\delta} \left(-\frac{1}{r}\int_0^r \frac{\partial u}{\partial z} r dr\right)\frac{\partial u}{\partial r} r dr = \tag{3.25}$$

$$-U_\infty \int_R^{R-\delta} \frac{\partial u}{\partial z} r dr - \int_R^{R-\delta} -\frac{\partial u}{\partial z} u r dr \tag{3.26}$$

Substituting the above equation back in equation (3.24) and flipping signs gives

$$\int_R^{R-\delta}\left[-u\frac{\partial u}{\partial z}+U_\infty\frac{\partial u}{\partial z}-u\frac{\partial u}{\partial z}+U_\infty\frac{dU_\infty}{dz}+u\frac{dU_\infty}{dz}-u\frac{dU_\infty}{dz}\right]rdr$$

$$=\int_R^{R-\delta}-\left[\frac{\tau_0}{\rho\, r_0}-\frac{1}{\rho r}\frac{\partial}{\partial r}(r\tau_{rz})\right]rdr \qquad (3.27)$$

Using algebraic manipulation, the above equation can be simplified to result in the integral form of the governing equation in the inlet region as shown below.

$$\int_R^{R-\delta}\left[\frac{\partial}{\partial z}[u(U_\infty-u)]+(U_\infty-u)\frac{dU_\infty}{dz}\right]rdr=\left[-\frac{\tau_0 r^2}{2\rho\, r_0}+\frac{(r\tau_{rz})}{\rho}\right]_R^{R-\delta} \qquad (3.28)$$

$$\int_R^{R-\delta}\left[\frac{\partial}{\partial z}(u(U_\infty-u)+(U_\infty-u)\frac{dU_\infty}{dz}\right]rdr$$

$$=-\frac{\tau_0[(R-\delta)^2+R^2]}{2\rho\, r_0}-\frac{R\tau_w}{\rho}+\frac{(R-\delta)\tau_0}{\rho} \qquad (3.29)$$

$$\int_R^{R-\delta}\left[\frac{\partial}{\partial z}[u(U_\infty-u)]+(U_\infty-u)\frac{dU_\infty}{dz}\right]rdr$$

$$=-\frac{\tau_0\left(\frac{\delta^2}{2}-R\delta\right)}{\rho\, r_0}+\frac{R\mu_o}{\rho}\left(\frac{\partial u}{\partial r}\right)_{r=R}-\frac{R\tau_0}{\rho}+\frac{(R-\delta)\tau_0}{\rho} \qquad (3.30)$$

3.2.4. Dimensionless form of the governing equation in the inlet region. Rearranging the above equation gives

$$R\frac{\partial}{\partial z}\left[U_\infty^2\int_0^\delta\frac{u}{U_\infty}\left(1-\frac{u}{U_\infty}\right)\left(1-\frac{y}{R}\right)(-dy)\right]$$

$$+RU_\infty\frac{dU_\infty}{dz}\int_0^\delta\left(1-\frac{u}{U_\infty}\right)\left(1-\frac{y}{R}\right)(-dy)$$

$$=-\frac{\tau_0\left(\frac{\delta^2}{2}-R\delta\right)}{\rho\, r_0}+\frac{R\mu_o}{\rho}\left(\frac{\partial u}{\partial r}\right)_{r=R}-\frac{R\tau_0}{\rho}+\frac{(R-\delta)\tau_0}{\rho} \qquad (3.31)$$

Using the definitions from Mohanty et al. [13] for the displacement thickness, equation (3.10), and the momentum thickness given below:

$$\delta^{**}\equiv\int_0^\delta\frac{u}{U_\infty}\left(1-\frac{u}{U_\infty}\right)\left(1-\frac{y}{R}\right)dy \qquad (3.32)$$

while substituting back in equation (3.31) yields

$$-R\frac{\partial}{\partial z}(U_\infty^2\delta^{**}) - RU_\infty\frac{dU_\infty}{dz}\delta^* = -\frac{\tau_0\left(\frac{\delta^2}{2}-R\delta\right)}{\rho\, r_0} + \frac{R\mu_o}{\rho}\left(\frac{\partial u}{\partial r}\right)_{r=R} - \frac{R\tau_0}{\rho} + \frac{(R-\delta)\tau_0}{\rho} \quad (3.33)$$

Using algebraic manipulation, the above equation can be expressed and simplified as

$$-R\left[2U_\infty\delta^{**}\frac{dU_\infty}{dz} + U_\infty^2\frac{d\delta^{**}}{dz}\right] - RU_\infty\delta^*\frac{dU_\infty}{dz} = -\frac{\tau_0\left(\frac{\delta^2}{2}-R\delta\right)}{\rho\, r_0} + \frac{R\mu_o}{\rho}\left(\frac{\partial u}{\partial r}\right)_{r=R} - \frac{R\tau_0}{\rho} + \frac{(R-\delta)\tau_0}{\rho} \quad (3.34)$$

$$-R\,U_\infty\frac{dU_\infty}{dz}(2\delta^{**}+\delta^*) - RU_\infty^2\frac{d\delta^{**}}{dz} = -\frac{\tau_0\left(\frac{\delta^2}{2}-R\delta\right)}{\rho\, r_0} + \frac{R\mu_o}{\rho}\left(\frac{\partial u}{\partial r}\right)_{r=R} - \frac{R\tau_0}{\rho} + \frac{(R-\delta)\tau_0}{\rho} \quad (3.35)$$

$$\frac{d\delta^{**}}{dz} + \frac{1}{U_\infty}\frac{dU_\infty}{dz}(2\delta^{**}+\delta^*) = \frac{\tau_0\left(\frac{\delta^2}{2}-R\delta\right)}{\rho\, r_0 U_\infty^2 R} - \frac{\mu_o}{U_\infty^2\rho}\left(\frac{\partial u}{\partial r}\right)_{r=R} + \frac{\tau_0}{U_\infty^2\rho} - \frac{(R-\delta)\tau_0}{U_\infty^2 R\rho} \quad (3.36)$$

Finally, the above equation can be further simplified by using the pressure gradient parameter defined earlier in equation (3.17).

$$\frac{d\delta^{**}}{dz} = -\frac{\mu_0}{\rho U_\infty}\left[\frac{1}{U_\infty}\left(\frac{\partial u}{\partial r}\right)_{r=R} + \frac{\lambda}{\delta^2}(2\delta^{**}+\delta^*)\right] - \frac{\tau_0\,\delta^2}{2\rho U_\infty^2 r_0 R} \quad (3.37)$$

Using the following dimensionless variables along with the ones defined in equation (3.13)

$$\bar{u} = \frac{u}{U_\infty} \qquad \eta = \frac{y}{\delta} \qquad \delta_1^{**} = \frac{\delta^{**}}{R}$$

$$\tau_0^* = \frac{\tau_0 R}{\mu_0 U_o} \qquad \tau_1 = \frac{\tau_o{}^*\delta_1{}^3}{1-\delta_1}\frac{U_o}{U_\infty} \qquad p^* = \frac{p}{\rho U_0^2/2} \quad (3.38)$$

and substituting in equation (3.37), results in the following dimensionless ordinary differential equation:

$$\frac{d\delta_1^{**}}{d\xi} = \frac{2\,U_0}{\delta_1 U_\infty}\left[-\left(\frac{\partial \bar{u}}{\partial \eta}\right)_{\eta=0} + \frac{\lambda}{\delta_1}(2\delta_1^{**} + \delta_1^{*}) + \frac{\tau_1}{2}\right] \tag{3.39}$$

This will be used along with equation (3.14) from the conservation of mass to solve for the velocity profile in the inlet region. The pressure gradient found in equation (3.22) can be expressed in dimensionless form as follows:

$$-\frac{dp^*}{d\xi} = \frac{4}{\delta_1^2}\frac{U_\infty}{U_0}\lambda + 4\frac{\tau_0^*}{r_0^*} \tag{3.40}$$

3.3. Governing Equations in the Filled Region

3.3.1. Boundary conditions in the filled region. We define Γ ($\mathbf{z}$) and $\boldsymbol{\lambda}$($\mathbf{z}$) as

$$\Gamma = \frac{\delta_e^2}{U_c}\left(\frac{\partial^2 u}{\partial r^2}\right)_{r=r_e} \tag{3.41}$$

$$\lambda = \delta_e^2 \frac{\rho}{\mu_0}\frac{dU_c}{dz}, \tag{3.42}$$

which extends the definitions used by Mohanty et al. [13] to Bingham fluid flow. In this region, the boundary layer thickness is a constant that depends on the fully developed plug-flow radius i.e. the yield stress of the fluid ($\delta = \delta_e = R - r_e = R - r_o =$ Constant). In order to reduce the number of symbols δ and r_o will be used.

The velocity profile satisfies the following boundary conditions

B.C. 1: at $r = R$ $\quad u = v = 0$

B.C.2: at $r = r_o$ $\quad u = U_c\,(z)$

B.C.3: at $r = r_o$ $\quad \dfrac{\partial u}{\partial y} = 0$ (3.43)

Similarly, applying equation (3.2) at the boundary layer's wall and edge while using the definition of λ, the fourth boundary condition B.C.4 becomes as follows

B.C.4: at $r = R$ $\quad \lambda - \Gamma = \delta_1 \dfrac{\partial \bar{u}}{\partial \eta} - \dfrac{\partial^2 \bar{u}}{\partial \eta^2} - \tau_1$ (3.44)

where $\bar{u} = u/U_c$ and $\tau_1 = \tau_o{}^* {\delta_1}^3/(1-\delta_1)\ U_o/U_c$.

3.3.2. Pressure gradient in the filled region. Following the same procedure used for the inlet region problem, and applying the momentum equation (3.2) at the edge of the boundary layer in the filled region yields

$$[u\frac{\partial u}{\partial z}+v\frac{\partial u}{\partial r}=-\frac{1}{\rho}\frac{dp}{dz}-\frac{1}{\rho r}\frac{\partial}{\partial r}(r\tau_{rz})]_{r=r_o} \tag{3.45}$$

Substituting τ_{rz} from equation (3.3) into the above equation and simplifying gives

$$U_c\frac{dU_c}{\partial z}=-\frac{1}{\rho}\frac{dp}{dz}-\left[\frac{1}{\rho r}\frac{\partial}{\partial r}\left(-r\mu_o\frac{\partial u}{\partial r}+r\tau_o\right)\right]_{r=r_o} \tag{3.46}$$

$$-\frac{1}{\rho}\frac{dp}{dz}=U_c\frac{dU_c}{\partial z}+\frac{\tau_0}{\rho\, r_0}-\frac{\mu_o}{\rho}\left(\frac{\partial^2 u}{\partial r^2}\right)_{r=r_o} \tag{3.47}$$

Rearranging the above equation, we can retrieve it in a form similar to the one in Mohanty et al. [13].

$$-\frac{\delta^2}{U_c\mu_o}\frac{dp}{dz}=\lambda-\Gamma+\frac{\tau_0^*\delta_1^2}{r_0^*}\left(\frac{U_o}{U_c}\right) \tag{3.48}$$

3.3.3. Integral form of the governing equation in the filled region. Similar to the methodology used for the inlet region, the von Kármán Pohlhausen scheme is adopted to obtain the solution for the boundary layer equation.

Substituting equation (3.47) into equation (3.2) results in

$$u\frac{\partial u}{\partial z}+v\frac{\partial u}{\partial r}=U_c\frac{dU_c}{dz}+\frac{\tau_0}{\rho\, r_0}-\frac{\mu_o}{\rho}\left(\frac{\partial^2 u}{\partial r^2}\right)_{r=r_o}-\frac{1}{\rho r}\frac{\partial}{\partial r}(r\tau_{rz}) \tag{3.49}$$

Rearranging equation (3.1) and substituting into (3.49) gives

$$u\frac{\partial u}{\partial z}+\left(-\frac{1}{r}\int_R^{R-\delta}\frac{\partial u}{\partial z}r dr\right)\frac{\partial u}{\partial r}$$
$$=U_c\frac{dU_c}{dz}+\frac{\tau_0}{\rho\, r_0}-\frac{\mu_o}{\rho}\left(\frac{\partial^2 u}{\partial r^2}\right)_{r=r_o}-\frac{1}{\rho r}\frac{\partial}{\partial r}(r\tau_{rz}) \tag{3.50}$$

The next step is to integrate from r = R at the wall to R = R - δ at the edge of the boundary layer. Integrating the second term by parts gives

$$\int_R^{R-\delta}\left(-\frac{1}{r}\int_R^{R-\delta}\frac{\partial u}{\partial z}rdr\right)\frac{\partial u}{\partial r}rdr$$
$$= -U_c\int_R^{R-\delta}\frac{\partial u}{\partial z}rdr - \int_R^{R-\delta} -\frac{\partial u}{\partial z}urdr\,. \qquad (3.51)$$

Substituting the above equation back in equation (3.50) and flipping signs gives

$$\int_R^{R-\delta}\left[-u\frac{\partial u}{\partial z}+U_c\frac{\partial u}{\partial z}-u\frac{\partial u}{\partial z}+U_c\frac{dU_c}{dz}+u\frac{dU_c}{dz}-u\frac{dU_c}{dz}\right]rdr$$
$$= \int_R^{R-\delta} -\left[\frac{\tau_0}{\rho\, r_0}-\frac{\mu_o}{\rho}\left(\frac{\partial^2 u}{\partial r^2}\right)_{r=r_o}-\frac{1}{\rho r}\frac{\partial}{\partial r}(r\tau_{rz})\right]rdr \qquad (3.52)$$

Following algebraic manipulation, the above equation can be simplified to result in the integral form of the governing equation in the filled region as shown below:

$$\int_R^{R-\delta}\left[\frac{\partial}{\partial z}(u(U_c-u)+(U_c-u)\frac{dU_c}{dz}\right]rdr$$
$$= \left[-\frac{\tau_0 r^2}{2\rho\, r_0}+\frac{\mu_o r^2}{2\rho}\left(\frac{\partial^2 u}{\partial r^2}\right)_{r=r_o}+\frac{(r\tau_{rz})}{\rho}\right]_R^{R-\delta} \qquad (3.53)$$

$$\int_R^{R-\delta}\left[\frac{\partial}{\partial z}(u(U_c-u)+(U_c-u)\frac{dU_c}{dz}\right]rdr$$
$$= -\frac{\tau_0((R-\delta)^2+R^2)}{2\rho\, r_0}+\frac{\mu_o((R-\delta)^2+R^2)}{2\rho}\left(\frac{\partial^2 u}{\partial r^2}\right)_{r=r_o}$$
$$-\frac{R\tau_w}{\rho}+\frac{(R-\delta)\tau_0}{\rho} \qquad (3.54)$$

$$\int_R^{R-\delta}\left[\frac{\partial}{\partial z}(u(U_c-u)+(U_c-u)\frac{dU_c}{dz}\right]rdr$$
$$= -\frac{\tau_0\left(\frac{\delta^2}{2}-R\delta\right)}{\rho\, r_0}+\frac{\mu_o\left(\frac{\delta^2}{2}-R\delta\right)}{\rho}\left(\frac{\partial^2 u}{\partial r^2}\right)_{r=r_o}$$
$$+\frac{R\mu_o}{\rho}\left(\frac{\partial u}{\partial r}\right)_{r=R}-\frac{R\tau_0}{\rho}+\frac{(R-\delta)\tau_0}{\rho} \qquad (3.55)$$

3.3.4. Dimensionless form of the governing equation in the filled region.

Rearranging the above equation yields

$$R\frac{\partial}{\partial z}\left[U_c^2\int_0^{\delta}\frac{u}{U_c}\left(1-\frac{u}{U_c}\right)\left(1-\frac{y}{R}\right)(-dy)\right] + RU_c\frac{dU_c}{dz}\int_0^{\delta}\left(1-\frac{u}{U_c}\right)\left(1-\frac{y}{R}\right)(-dy) = -\frac{\tau_0\left(\frac{\delta^2}{2}-R\delta\right)}{\rho\, r_0}+\frac{\mu_o\left(\frac{\delta^2}{2}-R\delta\right)}{\rho}\left(\frac{\partial^2 u}{\partial r^2}\right)_{r=r_o} + \frac{R\mu_o}{\rho}\left(\frac{\partial u}{\partial r}\right)_{r=R}-\frac{R\tau_0}{\rho}+\frac{(R-\delta)\tau_0}{\rho} \tag{3.56}$$

Using the following definitions from Mohanty et al. [13] for the displacement and momentum thicknesses

$$\delta^* \equiv \int_0^{\delta}\left(1-\frac{u}{U_c}\right)\left(1-\frac{y}{R}\right)dy \tag{3.57}$$

$$\delta^{**} \equiv \int_0^{\delta}\frac{u}{U_c}\left(1-\frac{u}{U_c}\right)\left(1-\frac{y}{R}\right)dy \tag{3.58}$$

and substituting in equation (3.56) yields

$$-R\frac{\partial}{\partial z}(U_c^2\delta^{**})-RU_c\frac{dU_c}{dz}\delta^* = -\frac{\tau_0\left(\frac{\delta^2}{2}-R\delta\right)}{\rho\, r_0}+\frac{\mu_o\left(\frac{\delta^2}{2}-R\delta\right)}{\rho}\left(\frac{\partial^2 u}{\partial r^2}\right)_{r=r_o} + \frac{R\mu_o}{\rho}\left(\frac{\partial u}{\partial r}\right)_{r=R}-\frac{R\tau_0}{\rho}+\frac{(R-\delta)\tau_0}{\rho} \tag{3.59}$$

Following algebraic manipulation, the above equation can be expressed as

$$-R\left[2U_c\delta^{**}\frac{dU_c}{dz}+U_c^2\frac{d\delta^{**}}{dz}\right]-RU_c\delta^*\frac{dU_c}{dz} = -\frac{\tau_0\left(\frac{\delta^2}{2}-R\delta\right)}{\rho\, r_0}+\frac{\mu_o\left(\frac{\delta^2}{2}-R\delta\right)}{\rho}\left(\frac{\partial^2 u}{\partial r^2}\right)_{r=r_o}$$

$$+\frac{R\mu_o}{\rho}\left(\frac{\partial u}{\partial r}\right)_{r=R}-\frac{R\tau_0}{\rho}+\frac{(R-\delta)\tau_0}{\rho} \tag{3.60}$$

$$-R\,U_c\frac{dU_c}{dz}(2\delta^{**}+\delta^{*})-RU_c^2\frac{d\delta^{**}}{dz}$$
$$=-\frac{\tau_0\left(\frac{\delta^2}{2}-R\delta\right)}{\rho\,r_0}+\frac{\mu_o\left(\frac{\delta^2}{2}-R\delta\right)}{\rho}\left(\frac{\partial^2 u}{\partial r^2}\right)_{r=r_o}$$
$$+\frac{R\mu_o}{\rho}\left(\frac{\partial u}{\partial r}\right)_{r=R}-\frac{R\tau_0}{\rho}+\frac{(R-\delta)\tau_0}{\rho} \tag{3.61}$$

$$\frac{d\delta^{**}}{dz}+\frac{1}{U_c}\frac{dU_c}{dz}(2\delta^{**}+\delta^{*})$$
$$=\frac{\tau_0\left(\frac{\delta^2}{2}-R\delta\right)}{\rho\,r_0U_c^2R}-\frac{\mu_o\left(\frac{\delta^2}{2}-R\delta\right)}{\rho U_c^2R}\left(\frac{\partial^2 u}{\partial r^2}\right)_{r=r_o}$$
$$-\frac{\mu_o}{U_c^2\rho}\left(\frac{\partial u}{\partial r}\right)_{r=R}+\frac{\tau_0}{U_c^2\rho}-\frac{(R-\delta)\tau_0}{U_c^2R\rho}. \tag{3.62}$$

Finally, the above equation can be further simplified by using the pressure gradient parameters defined earlier in equations (3.41) and (3.42).

$$\frac{d\delta^{**}}{dz}=-\frac{\mu_0}{\rho U_c}\left[\frac{1}{U_c}\left(\frac{\partial u}{\partial r}\right)_{r=R}+\frac{\lambda}{\delta^2}(2\delta^{**}+\delta^{*})+\frac{\Gamma}{\delta^2R}\left(\frac{\delta^2}{2}-R\delta\right)\right]$$
$$-\frac{\tau_0\,\delta^2}{2\rho U_c^2 r_o R} \tag{3.63}$$

Using the following dimensionless variables along with ones defined in equations (3.13) and (3.38)

$$\bar{u}=\frac{u}{U_c} \qquad\qquad \tau_1=\frac{\tau_o{}^*\delta_1{}^3}{1-\delta_1}\frac{U_o}{U_c} \tag{3.64}$$

and substituting in equation (3.63) results in the following dimensionless ordinary differential equation

$$\frac{d\delta_1^{**}}{d\xi}=-\frac{2\,U_0}{\delta_1 U_c}\left[-\left(\frac{\partial\bar{u}}{\partial\eta}\right)_{\eta=0}+\frac{\lambda}{\delta_1}(2\delta_1^{**}+\delta_1^{*})+\frac{\Gamma}{\delta_1}\left(\frac{\delta_1^2}{2}-\delta_1\right)+\frac{\tau_1}{2}\right] \tag{3.65}$$

The above equation will be used along with the conservation of mass equation (3.14) to solve for the velocity profile in the filled region.

The pressure gradient found in equation (3.48) can be expressed in dimensionless form as follows.

$$-\frac{dp^*}{d\xi} = \frac{4}{\delta_1^2}\frac{U_c}{U_0}(\lambda - \Gamma) + 4\frac{\tau_0^*}{r_0^*} \tag{3.66}$$

3.4. Skin-friction Coefficient

C_f is defined by the following expression [13]

$$C_f = \frac{\tau_w}{\rho U_o^2/2} \tag{3.67}$$

By applying equation (3.3) at the wall, the wall shear stress can be substituted in the above equation.

$$C_f = \frac{\tau_w}{\rho U_o^2/2} = \left[-\mu_0\left(\frac{\partial u}{\partial r}\right)_{r=R} + \tau_0\right]\frac{2}{\rho U_o^2}. \tag{3.68}$$

Substituting the dimensionless variables previously defined in equation (3.75) into the above equation and multiplying by Reynolds number result in

$$C_f Re = \left[\frac{U_c\mu_0}{\delta}\left(\frac{\partial \bar{u}}{\partial \eta}\right)_{\eta=0} + \frac{\tau_0^*\mu_0 U_o}{R}\right]\frac{2}{\rho U_o^2} * \frac{(2R)U_o\rho}{\mu_0} \tag{3.69}$$

$$\frac{1}{4}C_f Re = \frac{1}{\delta_1}\frac{U_c}{U_o}\left(\frac{\partial \bar{u}}{\partial \eta}\right)_{\eta=0} + \tau_0^*. \tag{3.70}$$

3.5. Fully Developed Flow

The velocity profile in the fully developed region is derived in many references including Ref. [18]. The plug-flow and outer-flow velocities are denoted as u_i and u_o, respectively.

The momentum equation is used to derive the pressure gradient as

$$\frac{1}{\rho}\frac{dp}{dz} = -\frac{1}{\rho r}\frac{\partial}{\partial r}(r\tau_{rz}) \tag{3.71}$$

Integrating the above equation and solving for τ_{rz} yields

$$\frac{dp}{dz} = -\frac{1}{r}\frac{\partial}{\partial r}(r\tau_{rz}) = C_o \tag{3.72}$$

$$\frac{1}{\rho}\frac{dp}{dz} = C_o \tag{3.73}$$

$$\frac{p_L - p_o}{L} = C_o \tag{3.74}$$

$$-\frac{1}{r}\frac{\partial}{\partial r}(r\tau_{rz}) = \frac{p_L - p_o}{L} \tag{3.75}$$

$$\frac{\partial}{\partial r}(r\tau_{rz}) = \frac{(p_o - p_L)}{L} r \tag{3.76}$$

$$\tau_{rz} = \frac{(p_o - p_L)}{2L} r \tag{3.77}$$

By applying the above equation at the wall, an expression for the wall shear stress is found.

$$\tau_w = \frac{(p_o - p_L)}{2L} R \tag{3.78}$$

Utilizing the following dimensionless variables

$$\Delta p^* = \frac{\Delta p}{\rho U_o^2/2}, \qquad \tau_w^* = \frac{\tau_w}{U_o \mu_0} R \tag{3.79}$$

equation (3.72) can be written as follows

$$\tau_w^* = \frac{\Delta p^*}{8\xi} \tag{3.80}$$

3.5.1. Outer-flow region. To obtain the velocity profile in the outer-flow region, equation (3.71) is combined with equation (3.3).

$$\tau_{rz} = \frac{(p_o - p_L)}{2L} r = \tau_0 - \mu_0 \frac{\partial u_o}{\partial r} \tag{3.81}$$

$$\frac{\partial u_o}{\partial r} = -\frac{(p_o - p_L)}{2L\mu_0} r + \frac{\tau_0}{\mu_0} \tag{3.82}$$

Integrating Eq. (3.82) gives

$$u_o = -\frac{(p_o - p_L)}{4L\mu_0} r^2 + \frac{\tau_0}{\mu_0} r + C_1 \tag{3.83}$$

The constant C_1 can be found by applying the no-slip boundary condition at the wall as follows:

$$\text{at } r = R \qquad u_o = 0 \tag{3.84}$$

$$0 = -\frac{(p_o - p_L)}{4L\mu_0}R^2 + \frac{\tau_0}{\mu_0}R + C_1 \tag{3.85}$$

$$C_1 = \frac{(p_o - p_L)}{4L\mu_0}R^2 - \frac{\tau_0}{\mu_0}R \tag{3.86}$$

By substituting the expression of the constant, the velocity profile in the outer-flow region is found as

$$u_o = -\frac{(p_o - p_L)}{4L\mu_0}r^2 + \frac{\tau_0}{\mu_0}r + \frac{(p_o - p_L)}{4L\mu_0}R^2 - \frac{\tau_0}{\mu_0}R \tag{3.87}$$

$$u_o = \frac{(p_o - p_L)}{4L\mu_0}R^2\left[1 - \left(\frac{r}{R}\right)^2\right] - \frac{\tau_0}{\mu_0}R\left[1 - \left(\frac{r}{R}\right)\right] \tag{3.88}$$

Using the previously defined dimensionless variables in equation (3.80), the outer-flow velocity profile can be expressed in a dimensionless form using the dimensionless shear stress at the wall.

$$\frac{u_o}{U_o} = \frac{\tau_w^*}{2}\left[1 - \left(\frac{r}{R}\right)^2\right] - \tau_0^*\left[1 - \left(\frac{r}{R}\right)\right] \tag{3.89}$$

3.5.2. Inner plug-flow region. Within the plug-flow region, the velocity profile is no longer a function of the radial co-ordinate and is a constant $\mathbf{C_2}$.

$$\frac{\partial u_i}{\partial r} = 0 \qquad 0 \le r \le r_o \tag{3.90}$$

$$u_i = C_2 \tag{3.91}$$

To obtain the outer-flow velocity profile, equations (3.77) and (3.3) are first combined

$$\tau_{rz} = \frac{(p_o - p_L)}{2L}r_o = \tau_0 \tag{3.92}$$

Using the above equation along with equation (3.80), a relationship between the yield stress and the wall shear stress is found.

$$\tau_0^* = \frac{\Delta p^*}{8\xi}r_o^* = \tau_w^* r_o^* \tag{3.93}$$

To obtain a continuous velocity profile, the velocity profiles of the plug-flow and boundary layer regions are equated at the edge of the boundary layer.

$$\text{at } r = r_o = r_e \qquad u_i = u_o \tag{3.94}$$

$$u_i = \frac{(p_o - p_L)}{4L\mu_0} R^2 \left[1 - \left(\frac{r_o}{R}\right)^2\right] - \frac{\tau_0}{\mu_0} R \left[1 - \left(\frac{r_o}{R}\right)\right] \tag{3.95}$$

Substituting equation (3.87) into equation (3.89) and simplifying the velocity profile expression gives

$$u_i = \frac{(p_o - p_L)}{4L\mu_0} R^2 \left[1 - \left(\frac{r_o}{R}\right)\right]^2. \tag{3.96}$$

Using the previously defined dimensionless variables in equations (3.80), the profile can be expressed in a dimensionless form using the wall shear stress.

$$\frac{u_i}{U_o} = \frac{\tau_w^*}{2} \left[1 - \left(\frac{r_o}{R}\right)\right]^2 \tag{3.97}$$

3.5.3. Other fully developed flow results. The results for the dimensionless fully developed centerline velocity, pressure gradient and plug flow radius are provided in [11] and are derived below. The provided velocity profiles can be re-written in terms of the yield stress using equation (3.93)

$$\frac{u_i}{U_o} = \frac{\tau_o^*}{2r_o^*} \left[1 - \left(\frac{r_o}{R}\right)\right]^2 \tag{3.98}$$

$$\frac{u_o}{U_o} = \frac{\tau_o^*}{2r_o^*} \left[1 - \left(\frac{r}{R}\right)^2\right] - \tau_o^* \left[1 - \left(\frac{r}{R}\right)\right] \tag{3.99}$$

A relationship between the yield stress and the plug flow radius can be found using the expression for the average velocity in the fully developed region.

$$U_o = \frac{1}{\pi R^2} \int_0^R 2\pi r u \, dr \tag{3.100}$$

$$\frac{U_o}{U_o} = \int_0^{r_o^*} 2 \frac{u_i}{U_o} r_1 dr_1 + \int_{r_o^*}^1 2 \frac{u_o}{U_o} r_1 dr_1 \tag{3.101}$$

$$= \frac{2\tau_o^*}{2r_o^*} (1 - r_o^*)^2 \int_0^{r_o^*} r_1 dr_1 + 2\tau_o^* \int_{r_o^*}^1 \frac{1}{2r_o^*} (r_1 - r_1^3) - (r_1 - r_1^2) \, dr_1 \tag{3.102}$$

$$= \frac{\tau_o^*}{r_o^*} (1 - r_o^*)^2 \left(\frac{r_o^{*2}}{2}\right) + \frac{\tau_o^*}{r_o^*} \left(\frac{1}{2} - \frac{r_o^{*2}}{2} - \frac{1}{4} + \frac{r_o^{*4}}{4}\right) - 2\tau_o^* \left(\frac{1}{2} - \frac{r_o^{*2}}{2} - \frac{1}{3} + \frac{r_o^{*3}}{3}\right) \tag{3.103}$$

$$\tau_0^* = \frac{12 r_o^*}{3 - 4r_o^* + r_o^{*4}} \tag{3.104}$$

By substituting equation (3.93) in the above equation, the pressure drop in the fully developed region can be found.

$$|\Delta p^*| = \frac{96\xi}{3 - 4r_e^* + r_e^{*4}} \tag{3.105}$$

The skin-friction coefficient in the fully developed region can be derived as follows using equation (3.93) and the definition of the coefficient from equation (3.67)

$$C_f Re = \frac{\tau_w}{\rho U_o^2/2} \frac{(2R)U_o\rho}{\mu_0} = 4\tau_w^* = 4\tau_0^*/r_o^* \tag{3.106}$$

For the Newtonian fully developed flow, where $\tau_0^* = r_o^* = 0$, the skin-friction coefficient can be found by taking the limit of the above equation.

$$C_f Re = \lim_{\tau_0^* \to 0} \frac{4\tau_0^*}{r_o^*} = \lim_{r_o^* \to 0} \left(\frac{4 * 12}{3 - 4r_o^* + r_o^{*4}} \right) = 16 \tag{3.107}$$

3.6. Solution

Following Mohanty and Asthana's [13] approach for Newtonian fluids, the following approximate quartic velocity profile is assumed in both the inlet and filled regions.

$$\bar{u} = \sum_{k=0}^{4} A_k(\lambda, \Gamma)\eta^k \tag{3.108}$$

By applying the boundary conditions in Sections 3.2.1 and 3.3.1, we retrieve the solution

$$\bar{u} = F(\eta) + \lambda_1 G(\eta) + \tau_2 G(\eta) + \Gamma_1 K(\eta) \tag{3.109}$$

where,

$$F(\eta) = 2\eta - 2\eta^3 + \eta^4 ,$$

$$G(\eta) = \frac{1}{6}(\eta - 3\eta^2 + 3\eta^3 - \eta^4) ,$$

$$K(\eta) = 3\eta^2 - 6\eta^3 + 3\eta^4 + \delta_1 \left(\frac{\eta^2}{2} - \eta^3 + \frac{\eta^4}{2} \right),$$

$$\lambda_1 = \frac{6(\lambda - 2\delta_1)}{6 + \delta_1}, \qquad \Gamma_1 = \frac{\Gamma}{6 + \delta_1}, \qquad \tau_2 = \frac{6\tau_1}{(6 + \delta_1)} \tag{3.110}$$

The coefficients A_k in the approximate velocity profile equation (3.100) are given below.

$$A_1 = (\lambda + \ \tau_1 + 12)/6 + \delta_1 \tag{3.111}$$

$$A_2 = (-6\lambda + 6\Gamma + 12\delta_1 - 6\tau_1 + \Gamma\delta_1)/[2(6 + \delta_1)] \tag{3.112}$$

$$A_3 = (-6\Gamma + 3\lambda \ - \ 8\delta_1 + \ 3\tau_1 - \ \Gamma\delta_1 \ - \ 12)/(6 + \delta_1) \tag{3.113}$$

$$A_4 = (6\Gamma - 2\lambda + 6\delta_1 - 2\tau_1 + \Gamma\delta_1 + 12)/[2(6 + \delta_1)] \tag{3.114}$$

For

$$\lambda_1 = \frac{-6(2\delta_1)}{6 + \delta_1}, \qquad \Gamma_1 = \frac{-2}{6 + \delta_1} \tag{3.115}$$

The velocity profile matches the fully developed one. Using the above polynomial expression, the displacement and momentum thicknesses are obtained as

$$\delta_1^* = \delta_1 \int_0^1 (1 - \bar{u})(1 - \delta_1\eta) \ d\eta \tag{3.116}$$

$$\delta_1^* = \delta_1 \int_0^1 [1 - \delta_1\eta] - \left[\sum A_k\eta^k - \delta_1 \sum A_k\eta^{k+1}\right] d\eta \tag{3.117}$$

$$\delta_1^* = \delta_1 \left[1 - \frac{\delta_1}{2}\right] - \delta_1 \left[\sum \frac{A_k}{k+1} - \delta_1 \sum \frac{A_k}{k+2}\right] \tag{3.118}$$

$$\delta_1^{**} = \delta_1 \int_0^1 \bar{u}(1 - \bar{u})(1 - \delta_1\eta) \ d\eta \tag{3.119}$$

$$\begin{aligned}\delta_1^{**} = \delta_1 \int_0^1 & \sum A_k\eta^k \\ & - \sum\sum A_kA_i\eta^{k+i}d\eta \\ & - \delta_1^2 \int_0^1 \sum A_k\eta^{k+1} - \sum\sum A_kA_i\eta^{k+i+1} \ d\eta\end{aligned} \tag{3.120}$$

$$\begin{aligned}\delta_1^{**} = \delta_1 & \left[\sum \frac{A_k}{k+1} - \sum\sum \frac{A_kA_i}{k+i+1}\right] \\ & - \delta_1^2 \left[\sum \frac{A_k}{k+2} - \sum\sum \frac{A_kA_i}{k+i+2}\right]\end{aligned} \tag{3.121}$$

3.6.1. Inlet region solution. Using equations (3.14) and (3.65), we can obtain the following pair of ordinary differential equations for δ_1 and λ using the chain rule with $\Gamma_1 = 0$

$$\frac{d\lambda}{d\xi} = \frac{\frac{d\delta_1^{**}}{d\xi} H_{1i} - \frac{d\delta_1^{*}}{d\xi} H_{3i}}{H_{1i}H_{4i} - H_{3i}H_{2i}} \tag{3.122}$$

$$\frac{d\delta_1}{d\xi} = \frac{\frac{d\delta_1^{*}}{d\xi} H_{4i} - \frac{d\delta_1^{**}}{d\xi} H_{2i}}{H_{1i}H_{4i} - H_{3i}H_{2i}} \tag{3.123}$$

where

$$H_{1i} = \frac{\partial \delta_1^*}{\partial \delta_1}; \qquad H_{2i} = \frac{\partial \delta_1^*}{\partial \lambda};$$

$$H_{3i} = \frac{\partial \delta_1^{**}}{\partial \delta_1}; \qquad H_{4i} = \frac{\partial \delta_1^{**}}{\partial \lambda}. \tag{3.124}$$

The initial conditions are $\lambda = \delta_1 = 0$ at $\xi = 0$.

3.6.2. Filled region solution. In the filled region, δ_1 is no longer a function of x and is equal to δ_e. Γ is now a variable, and we obtain the following differential equations for λ and Γ

$$\frac{d\lambda}{d\xi} = \frac{\frac{d\delta_1^{**}}{d\xi} H_{1f} - \frac{d\delta_1^{*}}{d\xi} H_{3f}}{H_{1f}H_{4f} - H_{3f}H_{2f}}, \tag{3.125}$$

$$\frac{d\Gamma}{d\xi} = \frac{\frac{d\delta_1^{*}}{d\xi} H_{4f} - \frac{d\delta_1^{**}}{d\xi} H_{2f}}{H_{1f}H_{4f} - H_{3f}H_{2f}}, \tag{3.126}$$

where,

$$H_{1f} = \frac{\partial \delta_1^*}{\partial \Gamma}; \qquad H_{2f} = \frac{\partial \delta_1^*}{\partial \lambda};$$

$$H_{3f} = \frac{\partial \delta_1^{**}}{\partial \Gamma}; \qquad H_{4f} = \frac{\partial \delta_1^{**}}{\partial \lambda}. \tag{3.127}$$

The initial conditions are $\Gamma = 0$ and the value of λ is reached at the end of the inlet region.

Chapter 4. Results and Discussion

Given a value of the yield-stress, equations (3.39) and (3.14) can be integrated to determine the profiles of δ_1 and λ_1 along the axial coordinate. Initially, both variables are zero at the inlet of the pipe. As described earlier, at the end of the inlet region, δ_1 should reach a limiting value depending on the yield stress, which is 1 for Newtonian fluids, and 1- r_e^* for Bingham fluids. In the filled region, δ_1 remains unchanged and the values for Γ_1 and λ_1 are obtained by integrating equations (3.66) and (3.14). The initial conditions are $\Gamma_1 = 0$, and the value of λ_1 is reached at the end of the inlet region. At the end of the filled region, the velocity profile reaches asymptotically the fully developed profile. For practicality, the end of the filled region is defined as the axial location where the centerline velocity reaches 99% of the fully developed value.

The present investigation is the first work applying the inlet-filled region momentum integral method to Bingham fluids originally developed for Newtonian fluids flow in circular pipes by Mohanty and Asthana [13]. The results are compared with the experimental data by Michiyoshi et al. [15] and the results obtained by Chen et al. [11] using the momentum integral and Campbell-Slattery methods.

As shown in Figure 4.1, the results for the boundary-layer thickness in the inlet region using the present work are in perfect agreement with the experimental data of Mohanty and Asthana [13] for Newtonian fluids. We can see from Figure 4.1 that the results of the momentum integral and Campbell-Slattery methods, as applied by Chen at al. [11], do not match the boundary-layer thickness experimental data for Newtonian fluid flow. Furthermore, Chen et al. [11] acknowledge that the results of the momentum integral method are unrealistic in regions far from the entry ($\xi > 0.02$).

Figure 4.2 shows the results for the boundary-layer thickness in the inlet region for various Bingham numbers. The higher the Bingham number, the smaller the inlet region length.

The results for λ and Γ are presented in Figures 4.3 and 4.4. As seen from the two figures, both parameters λ and Γ reach their asymptotic fully developed values of 0, and -2, respectively.

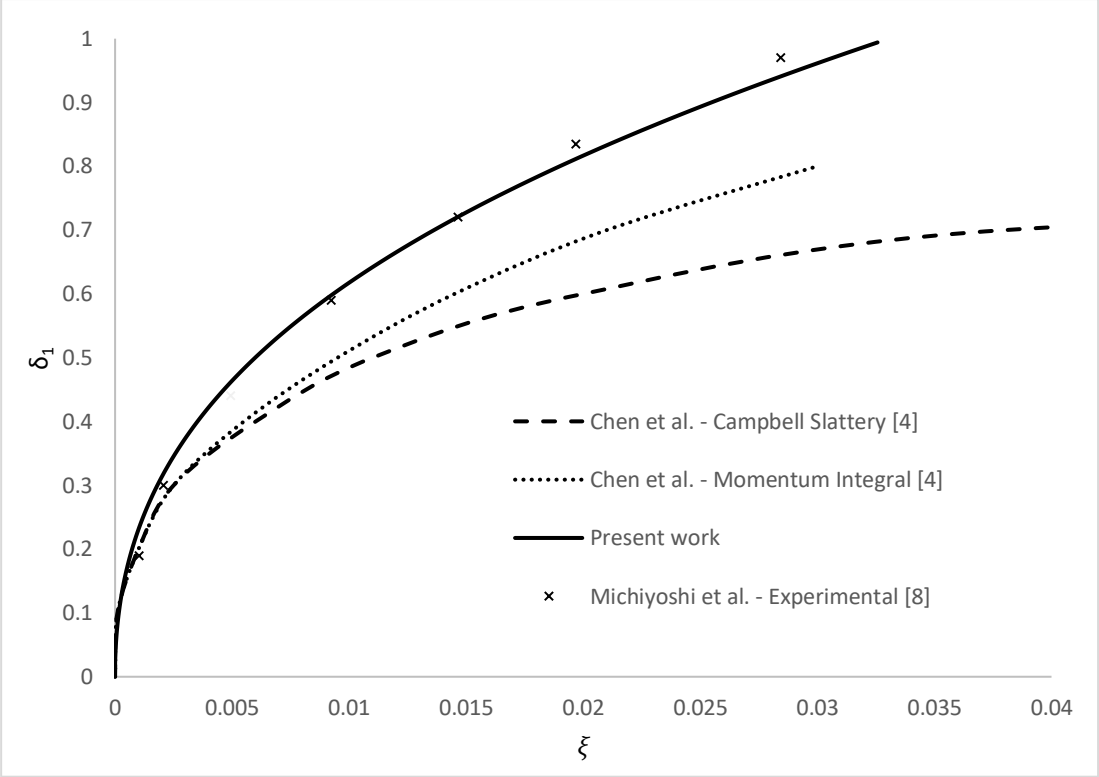

Figure 4.1: Boundary-layer thickness vs. axial location for $r_e^* = 0$.

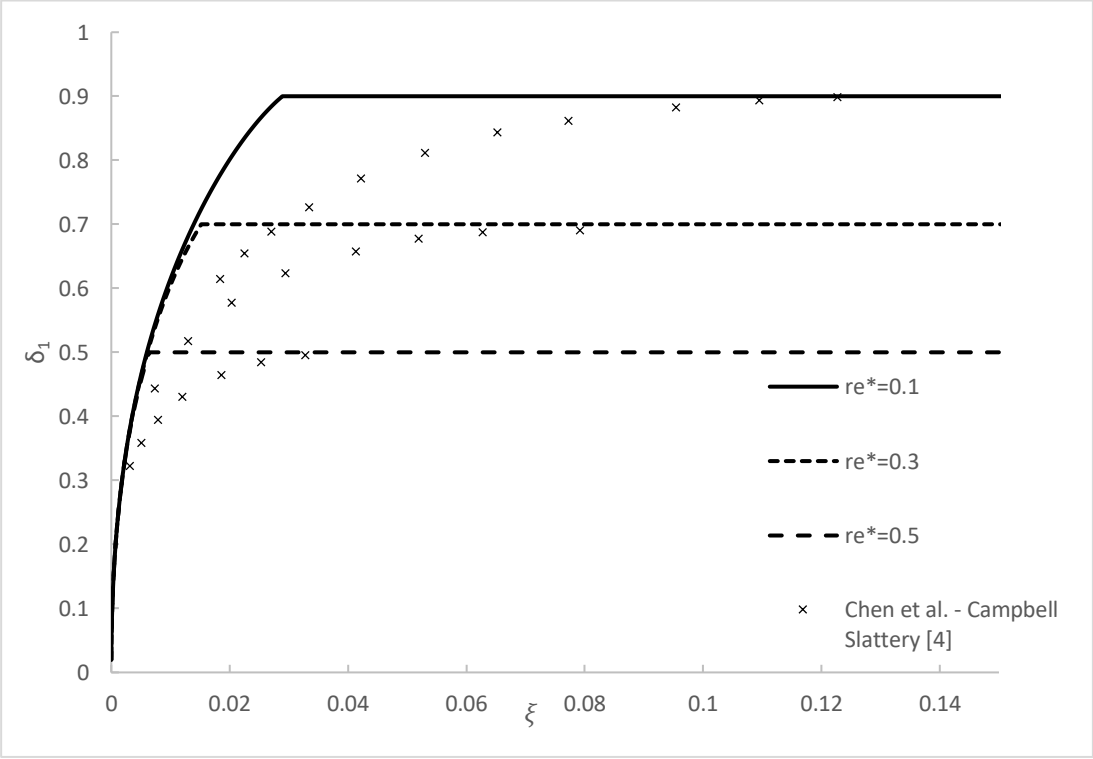

Figure 4.2: Boundary-layer thickness profiles for various Bingham numbers.

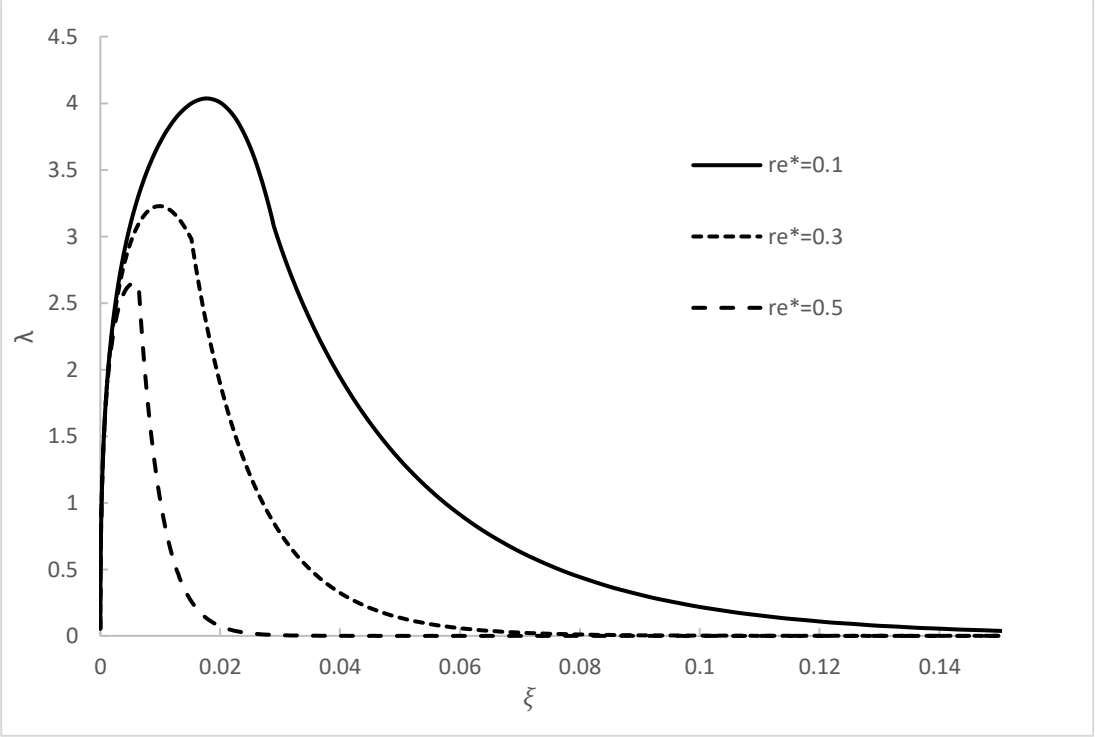

Figure 4.3: Profiles for λ.

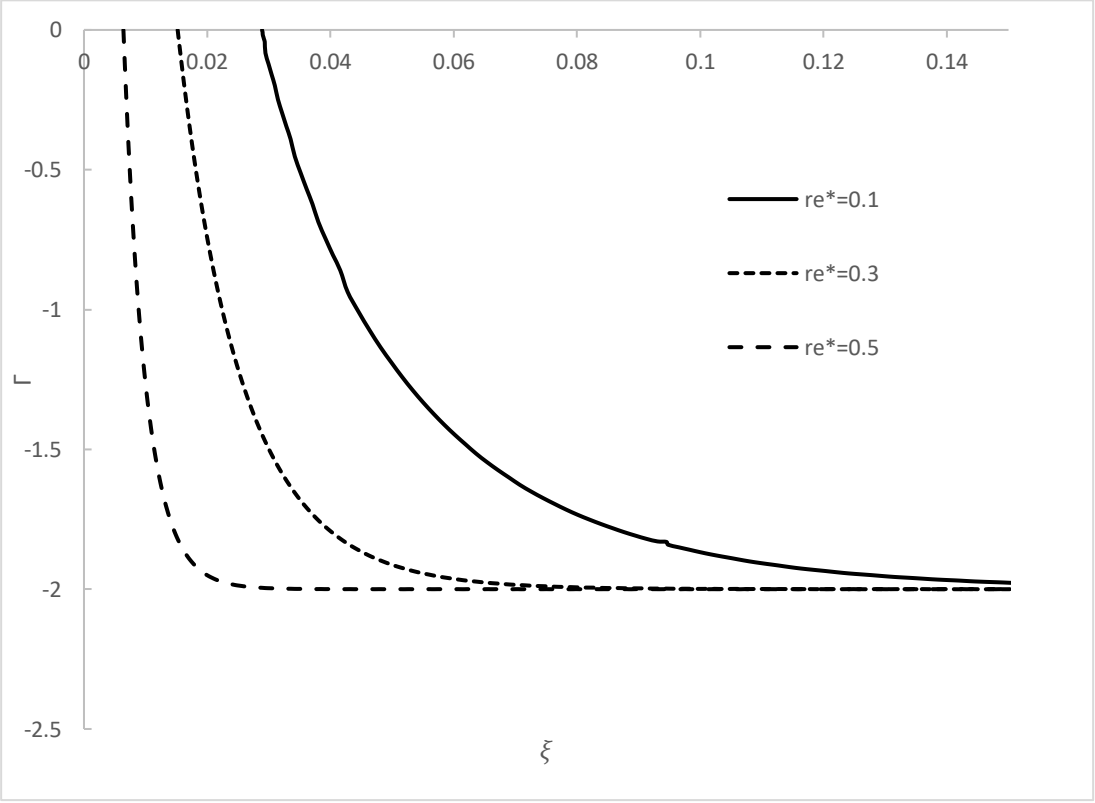

Figure 4.4: Profiles for Γ.

The results for pressure drop in the entrance region are presented in Figure 4.5 and Table 4.1, and are compared with the results of Chen et al. [11] and the experimental results by Michiyoshi et al. [15]. A better agreement is obtained with the present model.

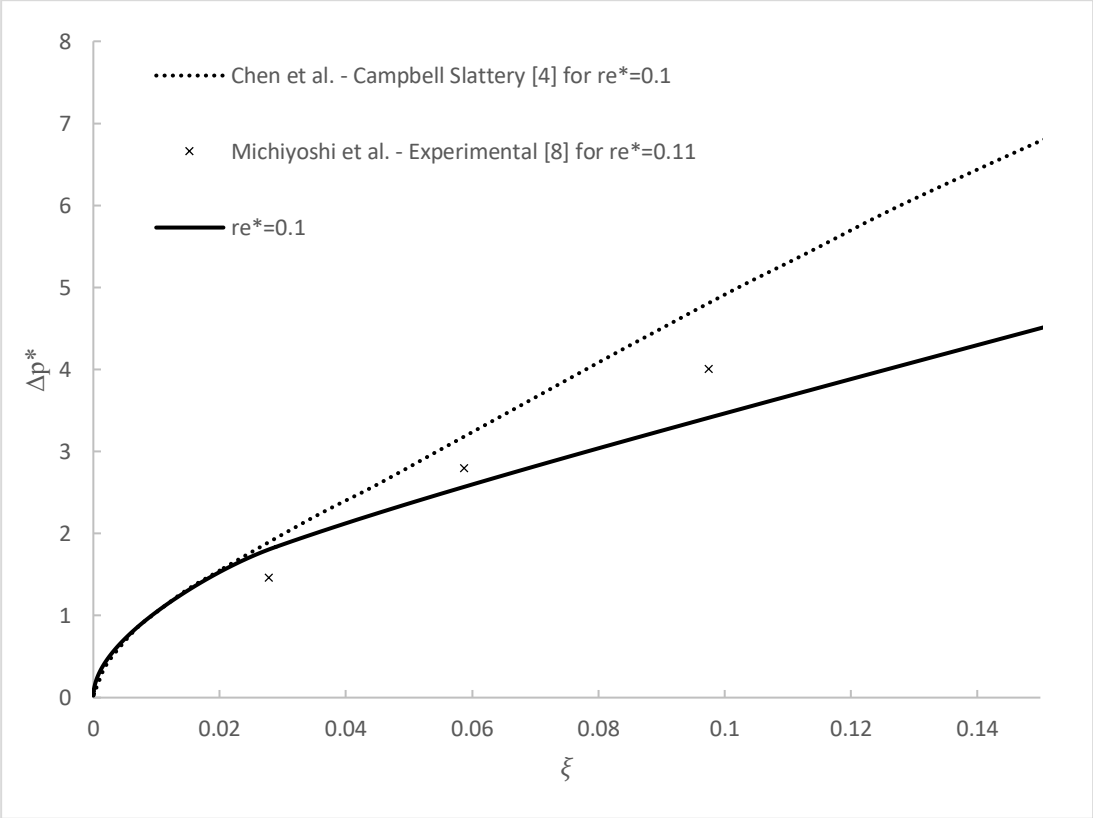

Figure 4.5: Pressure drop in the entrance region.

Table 4.1: Comparison of the pressure drop results in the entrance region.

ξ	Experimental pressure drop results [15]	Previous analytical pressure drop results [11]	Present work pressure drop results	%Error for previous analytical work	% Error for present work
0.0278	1.47	1.90	1.81	29.4	23.6
0.0588	2.80	3.50	2.56	25.0	8.48
0.0976	4.00	4.80	3.43	19.9	14.4

The velocity profiles are compared in Figure 4.6 with the results by Chen et al [11] using Campbell-Slattery method. As seen from the figure, results of the present work reach the fully developed values asymptotically.

Figure 4.7 compares the inlet and entrance region lengths with the results of Chen et al. [11]. The present results lie between the results by Chen et al. [11] using Campbell-Slattery and the momentum integral methods.

The fully developed pressure drop profiles are presented in Figure 4.8. Finally, the results for the skin-friction coefficient are presented in Figure 4.9. As seen from the figure, the results reach asymptotically the fully developed values.

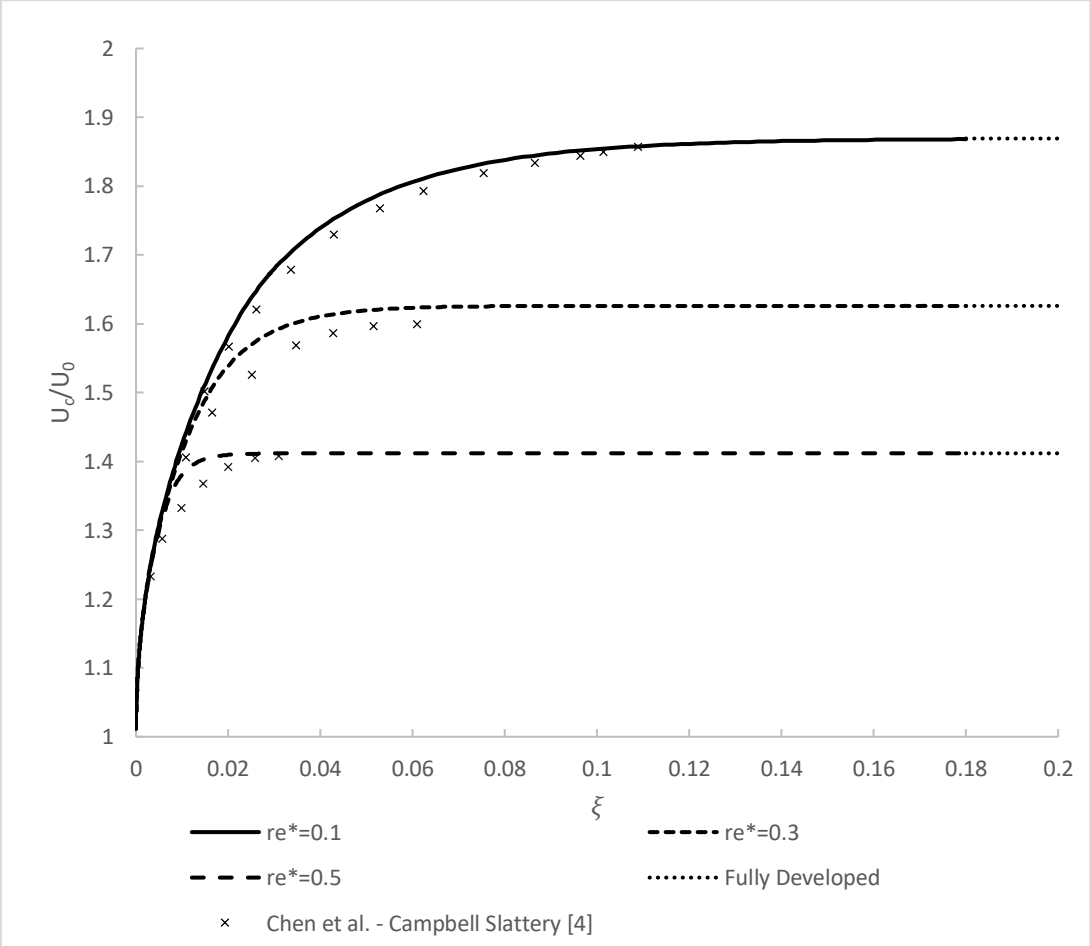

Figure 4.6: Centerline velocity profiles.

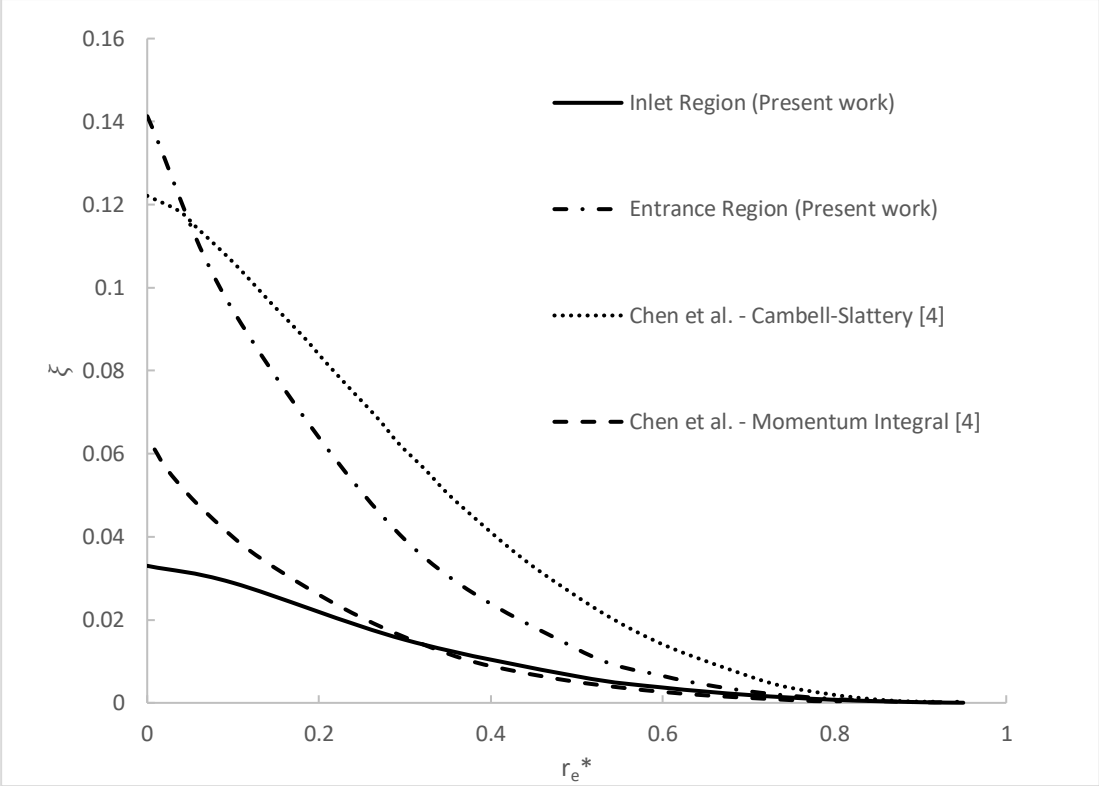

Figure 4.7: Inlet and entrance region lengths.

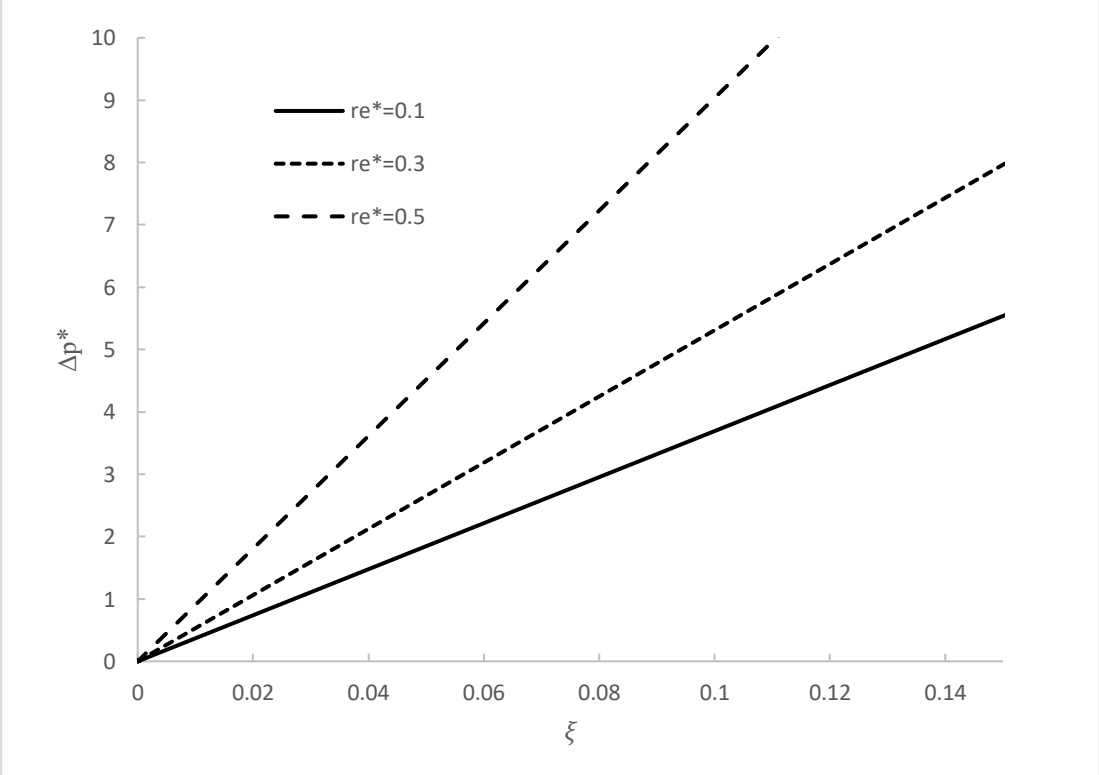

Figure 4.8: Fully developed pressure drop profiles.

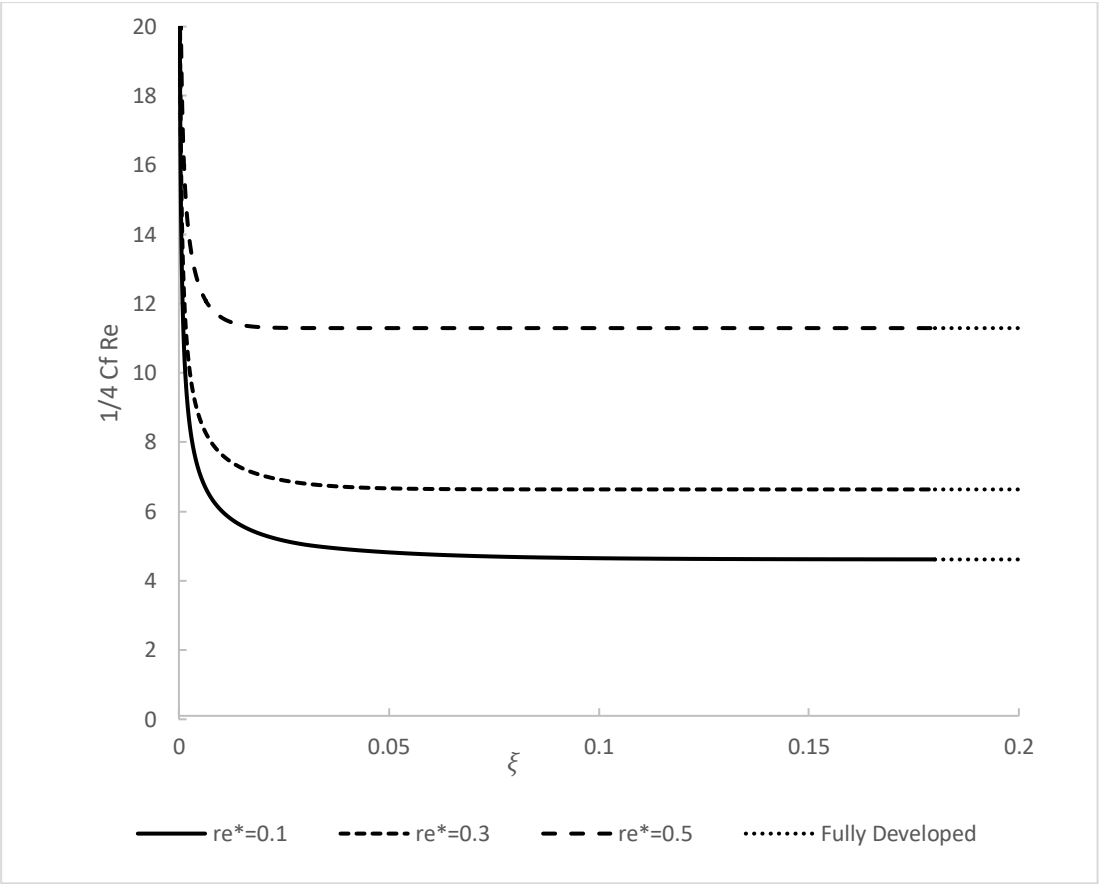

Figure 4.9: Skin-friction coefficient in the entrance region.

Chapter 5. Conclusions and Recommendations

5.1. Summary

Chapter 2 presented the results of the momentum integral method for Bingham fluid flow in a circular pipe using a quadratic profile as applied by Chen et al. [11]. Chapter 3 presented the current methodology of a modified momentum integral method using a quartic profile and including an additional filled region for Bingham fluids following Mohanty and Asthana's approach [13] for Newtonian fluids. The results are compared in Chapter 4 with experimental work [6, 8].

5.2. Conclusion

The isothermal laminar flow of a Bingham fluid in the entrance region of a circular pipe was studied using a modified momentum integral method that improves the previous boundary-layer model presented by Chen et al. [11]. The entrance region length and the velocity and pressure profiles were determined for various Bingham numbers. The results of Chen et al. [11] do not match the boundary-layer thickness experimental data for Newtonian fluid flow (yield stress equal to zero). The inconsistency is resolved in the present work using a quartic profile, while including an additional filled region following the inlet region, with both regions constituting the overall entrance region. The results obtained with the present model are in better agreement with the experimental pressure drop results by Michiyoshi et al. [15] as compared with the results obtained by Chen et al. [11].

5.3. Future work

Future research should include additional experimental work for further comparison with the boundary layer thickness, centerline velocity and pressure drop results presented in this work.

References

[1] H. Saffari, R. Moosavi, N. M. Nouri, and C.-X. Lin, “Prediction of hydrodynamic entrance length for single and two-phase flow in helical coils,” *Chemical Engineering and Processing: Process Intensification*, vol. 86, pp. 9–21, 2014.

[2] A. M. Teamah, M. A. Hassab, and W. M. El-Maghlany, “Influence of nano-particles addition on hydrodynamics and heat transfer in laminar flow entrance region inside tube,” *Alexandria Engineering Journal*, vol. 57, no. 4, pp. 4091–4102, 2018.

[3] M. Nobari and N. Nekoubin, “A numerical study of entrance region in a curved annulus with an inward and outward eccentricity,” *Engineering Science and Technology*, an International Journal, vol. 19, no. 3, pp. 1334–1345, 2016.

[4] M. Sahu, P. Singh, S. Mahapatra, and K. Khatua, “Prediction of entrance length for low Reynolds number flow in pipe using neuro-fuzzy inference system,” *Expert Systems with Applications*, vol. 39, no. 4, pp. 4545–4557, 2012.

[5] S. L. Kfuri, J. Q. Silva, E. J. Soares, and R. L. Thompson, “Friction losses for power-law and viscoplastic materials in an entrance of a tube and an abrupt contraction,” *Journal of Petroleum Science and Engineering*, vol. 76, no. 3-4, pp. 224–235, 2011.

[6] R. Chebbi, H. Al-Ali and M. Sami Selim, "Simultaneously developing laminar flow and heat transfer in the entrance region of a circular tube with constant wall temperature," *Chemical Engineering Communications*, vol. 160, no. 1, pp. 59-70, 1997.

[7] S. R. Nadiminti and A. Kandasamy, “Entrance region flow in concentric annuli with rotating inner wall for Bingham fluid,” *Journal of Computational and Applied Mechanics*, vol. 11, no. 2, pp. 137–157, 2016.

[8] R. Poole and R. Chhabra, "Development length requirements for fully developed laminar pipe flow of yield stress fluids," *Journal of Fluids Engineering*, vol. 132, no. 3, p. 034501, 2010.

[9] N. De Nevers, *Fluid Mechanics for Chemical Engineers*, McGraw Hill, 2005.

[10] R. B. Bird, W. E. Stewart, and E. N. Lightfoot, *Transport Phenomena*. Wiley, 2007.

[11] S. Chen, L. Fan and C. Hwang, "Entrance region flow of the Bingham fluid in a circular pipe," *AIChE Journal*, vol. 16, no. 2, pp. 293-299, 1970.

[12] S. Ishizawa, "The axi-symmetric laminar flow in an arbitrarily shaped narrow gap : (2nd Report, Theoretical analysis for the downstream region)," *Bulletin of JSME*, vol. 9, no. 33, pp. 86-103, 1966.

[13] A. Mohanty and S. Asthana, "Laminar flow in the entrance region of a smooth pipe," *Journal of Fluid Mechanics*, vol. 90, no. 03, p. 433, 1979.

[14] R. Chebbi, "Laminar flow of power-law fluids in the entrance region of a pipe, " *Chemical Engineering Science*, vol. 57, no. 21, pp. 4435-4443, 2002.

[15] L. Michiyoshi, K. Mizuno, Y. Hoshiai, “Studies on the flow of slurry through a pipe. I. Entrance region of laminar flow,” *International Chemical Engineering*, vol. 6, no. 2, pp. 373-381, 1966.

[16] L. Schiller, "Die Entwicklung der laminaren Geschwindigkeitsverteilung und ihre Bedeutung für Zähigkeitsmessungen., (Mit einem Anhang über den Druckverlust turbulenter Strömung beim Eintritt in ein Rohr.)," *ZAMM* -

Zeitschrift für Angewandte Mathematik und Mechanik, vol. 2, no. 2, pp. 96-106, 1922.

[17] W. D. Campbell, and J. C. Slattery, "Flow in the entrance of a tube*," American Society of Mechanical Engineers Transactions Series D*, vol. 85, pp. 41-44, 1963.

[18] V. Shah and R. Soto, "Entrance flow of a bingham fluid in a tube," *Applied Scientific Research*, vol. 30, no. 4, pp. 271-278, 1975.

[19] S. V. Patankar and D. B. Spalding, "A calculation procedure for heat, mass and momentum transfer in three-dimensional parabolic flows," *International Journal of Heat and Mass Transfer*, vol. 15, no. 10, pp. 1787–1806, 1972.

[20] Z. Nowak and B. Gajdeczko, "Laminar entrace region flow of the Bingham fluid," Acta Mechanica, vol. 49, no. 3-4, pp. 191-200, 1983.

[21] Z. Matras and J. Stachura, "Laminarny przeplyw cieczy newtonowskiej w obszarze wlotowym rury kolowej," *Archiwum Hydrotechniki*, vol. 28, no. 2, 1981.

[22] G. Vradis, J. Dougher and S. Kumar, "Entrance pipe flow and heat transfer for a Bingham plastic," *International Journal of Heat and Mass Transfer*, vol. 36, no. 3, pp. 543-552, 1993.

[24] S. Ookawara, K. Ogawa, N. Dombrowski, E. Amooie-Foumeny and A. Riza, "Unified entry length correlation for Newtonian, power law and Bingham fluids in laminar pipe flow at low Reynolds number," *Journal of Chemical Engineering of Japan*, vol. 33, no. 4, pp. 675-678, 2000.

[25] M. Al Khatib and S. Wilson, "The development of Poiseuille flow of a yield-stress fluid," *Journal of Non-Newtonian Fluid Mechanics*, vol. 100, no. 1-3, pp. 1-8, 2001.

Vita

Basma Baioumy was born in 1991, in Dubai, United Arab Emirates. She received her primary and secondary education in the UAE. She received her B.Sc. degree in chemical engineering from the American University of Sharjah in 2011. From 2012 to 2015, she worked as a Wireline Field Engineer for Baker Hughes Inc. In September 2015, she joined the chemical engineering master's program at the American University of Sharjah as a graduate teaching assistant. During her master's study, she presented a synopsis of this research at the Graduate Student Research Conference (March 20, 2017, Khalifa University, Abu Dhabi). From 2017 to 2019, she worked as a Regional Technical Advisor in TAM International.

Her research interests are in fluid dynamics, computing and simulation, energy and sustainability, materials and nanoengineering, and production and reservoir enhancement.